



# CHORUS

This is the accepted manuscript made available via CHORUS. The article has been published as:

## Chirality Memory Stored in Magnetic Domain Walls in the Ferromagnetic State of MnP

N. Jiang, Y. Nii, H. Arisawa, E. Saitoh, J. Ohe, and Y. Onose

Phys. Rev. Lett. **126**, 177205 — Published 28 April 2021

DOI: [10.1103/PhysRevLett.126.177205](https://doi.org/10.1103/PhysRevLett.126.177205)

# Chirality memory stored in magnetic domain walls in the ferromagnetic state of MnP

N. Jiang<sup>1,\*</sup>, Y. Nii<sup>2,3</sup>, H. Arisawa<sup>2</sup>, E. Saitoh<sup>2,4,5,6</sup>, J. Ohe<sup>7</sup>, and Y. Onose<sup>2</sup>

<sup>1</sup>*Department of Basic Science, The University of Tokyo, Tokyo 153-8902, Japan.*

<sup>2</sup>*Institute for Materials Research, Tohoku University, Sendai 980-8577, Japan.*

<sup>3</sup>*PRESTO, Japan Science and Technology Agency (JST), Kawaguchi 332-0012, Japan.*

<sup>4</sup>*Department of Applied Physics, The University of Tokyo, Tokyo 113-8656, Japan.*

<sup>5</sup>*Advanced Science Research Center, Japan Atomic Energy Agency, Tokai 319-1195, Japan.*

<sup>6</sup>*Advanced Institute for Materials Research, Tohoku University, Sendai 980-8577, Japan.*

<sup>7</sup>*Department of Physics, Toho University, 2-2-1 Miyama, Funabashi 274-8510, Japan.*

(Dated: March 31, 2021)

Chirality in a helimagnetic structure is determined by the sense of magnetic moment rotation. We found that the chiral information did not disappear even after the phase transition to the high-temperature ferromagnetic phase in a helimagnet MnP. The 2nd harmonic resistivity  $\rho^{2f}$ , which reflects the breaking down of mirror symmetry, was found to be almost unchanged after heating the sample above the ferromagnetic transition temperature and cooling it back to the helimagnetic state. The application of a magnetic field along the easy axis in the ferromagnetic state quenched the chirality-induced  $\rho^{2f}$ . This indicates that the chirality memory effect originated from the ferromagnetic domain walls.

Chirality is a lack of mirror symmetry in matter. When some matter has chirality, its mirror image is different from the original. In other words, there exist two distinguishable states (enantiomers) in the chiral matters. The concept is valid in various scientific fields ranging from high-energy physics to biology. For example, the homo-chiral state in living bodies has been attracted much attention. It has been extensively studied how the chiral information is transferred and memorized[1, 2].

Chirality also appears in magnetic structures. A representative example is a helical magnetic structure, in which the ordered direction of the magnetic moment spatially rotates in a plane perpendicular to the propagation vector (Fig. 1(c)). The sense of rotation is reversed by any mirror operation and therefore determines the chiral state. The helimagnets have been attracting great attention recently because they in some cases show the topological spin textures denoted as skyrmion lattice and soliton lattice in a magnetic field, which gives rise to unconventional magnetoelectric coupling[3–5]. What is more important here is that the helical magnets can work as toy models of general chirality problems because magnetic moments are stable and well controllable objects, and can be extensively investigated in a small laboratory. In this paper, we report an interesting phenomenon related to magnetic chirality; the information of the chirality in a helical magnetic phase is memorized even in a nonchiral ferromagnetic phase at a higher temperature in an itinerant helimagnet MnP. MnP has a centrosymmetric crystal structure (Fig. 1(a))[6–13]. While the sense of spin rotation is fixed by the crystal chirality in helimagnets with the chiral crystal structure, it can be viewed as a degree of freedom in this material. Similar memory effects of spin rotation direction were observed in multiferroic spiral magnets with polar symmetry[14–21] and

the origin was, in many cases, ascribed to so-called polar nanoregion or charge related effects. In the present case, there is no obvious coupling to the electric fields because the magnetic structure belongs to chiral symmetry. Here we show how the chirality of the helical magnet is memorized in an achiral ferromagnetic state, which seems valuable information even in the context of the general chirality problem.

Figure 1(b) shows the phase diagram of MnP, which was constructed based on magnetoresistance measurements of a microscale sample ( $10 \times 20 \times 1 \mu\text{m}^3$ ) fabricated for the present study by using the focused ion beam technique [22]. It is quite similar to that of a bulk sample reported in a previous study[13]. The ferromagnetically ordered phase (FM1) was stable even at zero magnetic field above 60 K, and the magnetic moments aligned along the  $c$ -axis (Fig. 1(d)). In this magnetic state, chiral Bloch-type magnetic domain walls were observed by Lorentz transmission electron microscopy[10]. The sense of spin rotation corresponds to chirality similarly to the case of helimagnetic structure. On the other hand, in the helimagnetic state (HEL), which showed up below 44 K, the helical plane was normal to the propagation vector along the  $a$ -axis[9] (Fig. 1(c)). The intermediate hatched region indicates the metastable region typical of the first-order phase transition. When the magnetic field was applied parallel to the  $a$ -axis in the helimagnetic state, the magnetic moments were tilted, forming a conical magnetic state (CON) (Fig. 1(e)). As the magnetic field increased further before the magnetic moments became completely aligned along the  $a$ -axis (FM2), there emerged a fan structure (FAN), in which the magnetic moments were within the  $ac$  plane, and the angle between the magnetic moment and the propagation vector spatially oscillated along the propagation vector (Fig. 1(f)). In our previous work[23], we controlled the chirality of the helimagnetic structure by the simultaneous application of a magnetic field and a dc electric current and probed the

---

\* jiangnan@g.ecc.u-tokyo.ac.jp

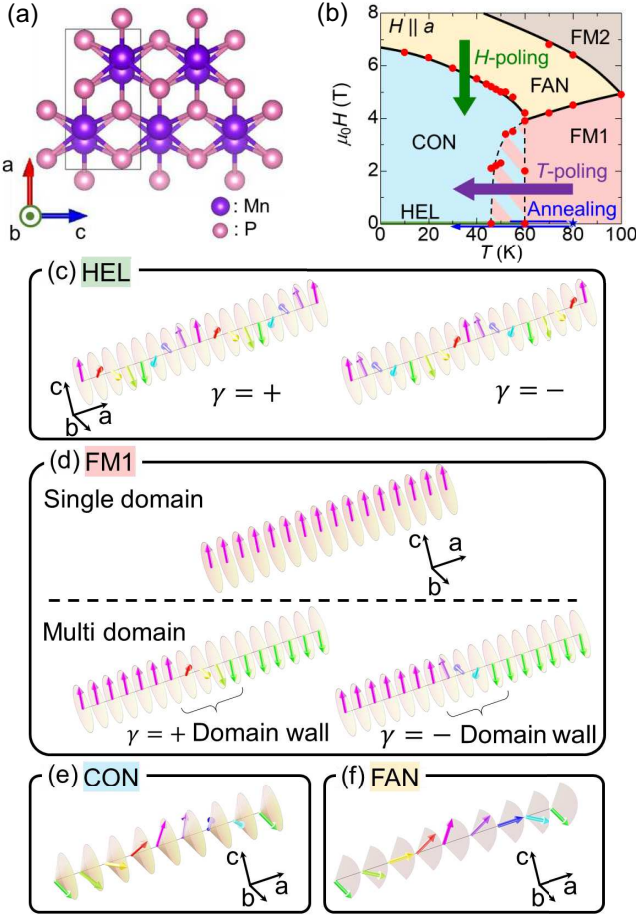


FIG. 1. (a) Crystal structure of MnP. The black line represents the unit cell. (b) The phase diagram of a micro-fabricated MnP sample for  $H \parallel a$ . The dots are the phase boundaries estimated by the magnetic field dependence of the electrical resistivity[22]. The dashed and solid lines are guides for the eyes. In the hatched region, the realized magnetic structure depends on the hysteresis. The arrows illustrate the  $H$ -poling,  $T$ -poling and annealing procedures (see main text). (c) Illustrations of helical magnetic structures.  $\gamma = \pm$  denotes the chirality. (d) Illustrations of ferromagnetic structure and Bloch-type ferromagnetic domain walls. (e),(f) Illustrations of conical and fan magnetic structures.

controlled chirality by the nonreciprocal electronic transport, which is the field asymmetric component of 2nd harmonic resistivity[24–27]. The controlled chirality was shown to be dependent on whether the applied magnetic field and the dc electric current are parallel or antiparallel to each other. In this paper, we show how the controlled chirality in the helimagnetic state was preserved or disappeared in the high-temperature ferromagnetic state.

To reveal how the chirality information is affected by external stimuli in the course of phase transitions, we show the field-asymmetric 2nd harmonic resistivity after the simultaneous application of a magnetic field and a dc electric current in the course of FAN-to-CON and FM1-to-CON phase transitions. For the FAN-to-CON transi-

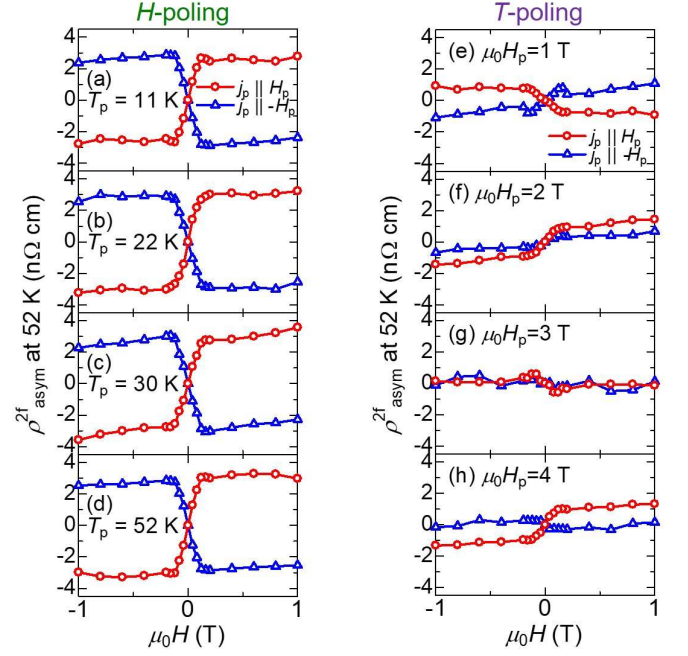


FIG. 2. (a)-(d) Magnetic field dependence of  $\rho_{\text{asym}}^{2f} = (\rho^{2f}(H) - \rho^{2f}(-H))/2$  at 52 K after the  $H$ -poling procedure performed at (a)  $T_p = 11$  K, (b) 22 K, (c) 30 K and (d) 52 K with dc electric currents  $j_p$  parallel to and anti-parallel to magnetic fields  $H_p$ . The magnitude of  $j_p$  was  $4.2 \times 10^8$  Am $^{-2}$  at 11 K and  $8.5 \times 10^8$  Am $^{-2}$  at 22 K, 30 K and 52 K. The magnitude of ac electric current for measuring the 2nd harmonic resistivity  $j_{ac}$  was  $5.9 \times 10^8$  Am $^{-2}$ . (e)-(h) Magnetic field dependence of  $\rho_{\text{asym}}^{2f}$  at 52 K after the  $T$ -poling procedure at (e)  $\mu_0 H_p = 1$  T, (f) 2 T, (g) 3 T and (h) 4 T with  $j_p \parallel H_p$  and  $j_p \parallel -H_p$ . The magnitudes of  $j_p$  and  $j_{ac}$  were  $8.5 \times 10^8$  Am $^{-2}$  and  $5.9 \times 10^8$  Am $^{-2}$ , respectively.

tion, we applied a dc electric current  $j_p$  parallel or antiparallel to the magnetic field  $H_p$  along the propagation vector ( $a$ -axis) when the FAN-to-CON transition field was traversed. The magnitude of  $\mu_0 H_p$  was slowly decreased from 7 T to 4 T at a rate of 0.6 Tmin $^{-1}$ . Then, we removed the dc electric current  $j_p$ . We call the series of these processes the “ $H$ -poling procedure”(Fig. 1(b)). In our previous paper[23], we performed the  $H$ -poling procedure at 51 K and measured the 2nd harmonic resistivity to show the chirality control. Here we performed the  $H$ -poling procedure at various temperatures and measured the 2nd harmonic resistivity at the same temperature, 52 K. Figures 2(a)-2(d) show the asymmetric component of the 2nd harmonic resistivity  $\rho_{\text{asym}}^{2f} = (\rho^{2f}(H) - \rho^{2f}(-H))/2$  at 52 K after the  $H$ -poling at various temperatures  $T_p$ . Here  $\rho^{2f}$  is the observed 2nd harmonic resistivity. As discussed in the previous paper[23],  $\rho_{\text{asym}}^{2f}$  is sensitive to the breaking of chiral symmetry, whereas the symmetric component seems to be due to sample nonuniformity and/or electrode contact. Notable  $\rho_{\text{asym}}^{2f}$  was discerned for all the poling conditions. The signal was reversed by the reversal of the dc poling electric current.

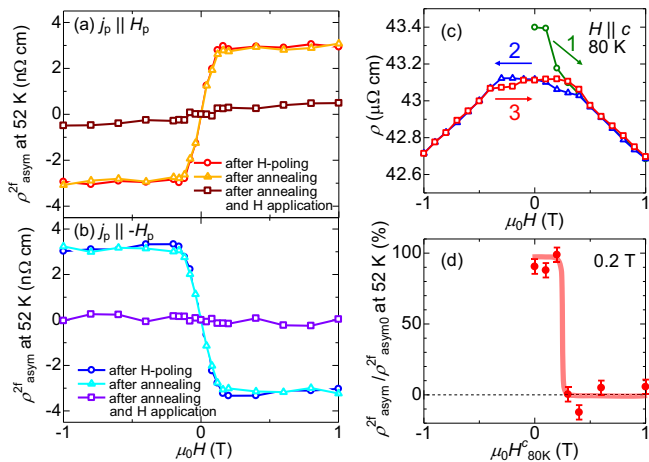


FIG. 3. (a),(b) Magnetic field dependence of  $\rho^{2f}_{\text{asym}}$  at 52 K at the initial state (just after H-poling, circles), that after annealing at 80 K (triangles), and that after annealing at 80 K and application of 1 T magnetic field along the  $c$ -axis (squares). The initial  $\rho^{2f}_{\text{asym}}$  was positive ( $j_p \parallel H_p$ ) and negative ( $j_p \parallel -H_p$ ) in (a) and (b), respectively. (c) Magnetic field dependence of the resistivity  $\rho$  at 80 K. The magnetic field was parallel to the magnetic easy axis ( $c$ -axis). Circles represent the data measured just after a phase transition from the helical to the ferromagnetic phase at 0 T. Triangles and squares represent the resistivity measured while decreasing the magnetic field from 1 T to -1 T and while increasing the magnetic field from -1 T to 1 T, respectively. (d)  $\rho^{2f}_{\text{asym}}$  at 0.2 T measured after annealing and application of magnetic field  $H^c_{80K}$  normalized by that before the annealing process ( $\rho^{2f}_{\text{asym}0}$ ) plotted against  $\mu_0 H^c_{80K}$ . The magnetic field  $H^c_{80K}$  was applied along the  $c$ -axis at 80 K. The error bar is estimated as the standard deviation of  $\rho^{2f}_{\text{asym}} / \rho^{2f}_{\text{asym}0}$  for the  $\mu_0 H^c_{80K} = 1$  T data (Fig. 3(b) squares), which is assumed to vanish.

These features indicate that the chirality is effectively controlled by the application of the electric current and the magnetic field in the course of the FAN-CON transition, irrespective of temperature.

While the FAN-CON transition is a second-order phase transition, the FM1-CON transition is a first order one. In the former case, the magnetic structural change is continuous and the susceptibility relevant to the symmetry breaking diverges at the critical point. On the other hand, in the latter case, the magnetic structural change is discontinuous. For this reason, the chirality responses in the course of these phase transitions were quite different. We tried to control the chirality by a similar poling procedure via the FM1-CON transition (Fig. 1(b)). We applied  $j_p$  parallel or antiparallel to  $H_p$  along the  $a$ -axis when the transition temperature was traversed. The temperature was slowly decreased from 80 K to 30 K at a rate of  $0.5 \text{ Kmin}^{-1}$  with a constant magnitude of  $H_p$ . Then, we removed  $j_p$ . We call the series of these processes the “ $T$ -poling procedure”. Figures 2(e)-2(h) show  $\rho^{2f}_{\text{asym}}$  at 52 K after  $T$ -poling procedures at various  $H_p$ . The magnitude was much smaller than the case of the  $H$ -poling. It

should be noted that the signal was not reproducible[22]. These features indicate that the  $T$ -poling is not effective for chirality control. The critical enhancement of susceptibility in the course of second-order phase transition seems essential to control the chirality.

Thus, the chirality was insensitive to the external stimuli when traversing the first-order FM1-CON transition. We also found that the chiral information was preserved through this phase transition at zero magnetic field, as shown below. In Figs. 3(a) and 3(b), we show  $\rho^{2f}_{\text{asym}}$  just after the  $H$ -poling and that after the  $H$ -poling and the subsequent annealing process (heating up to 80 K, cooling down to 30 K, and going back to the original measuring temperature of 52 K, as shown in Fig. 1(b)). The  $\rho^{2f}_{\text{asym}}$  signal was almost unchanged even after the annealing process, irrespective of the sign of  $\rho^{2f}_{\text{asym}}$ . This observation suggests that the chiral information is preserved even in the FM1 phase at zero field. Then, the question is how the chiral information is preserved in the collinear ferromagnet. This can be answered by considering the effect of magnetic field application along the magnetic easy axis ( $c$ -axis) at 80 K. After heating the sample up to 80 K, we rotated the sample device in the superconducting magnet and applied a magnetic field  $\mu_0 H^c_{80K}$  as large as 1 T along the  $c$ -axis. Then, we decreased the temperature to 30 K at 0 T and increased it again to the original measuring temperature of 52 K. Figures 3(a) and 3(b) also show  $\rho^{2f}_{\text{asym}}$  at 52 K after this annealing process with the application of a magnetic field  $H^c_{80K}$ . It is clear from this figure that the  $\rho^{2f}_{\text{asym}}$  signal was quenched by the application of  $H^c_{80K}$ . This result implies that it is the ferromagnetic domain walls that memorize the chiral information. While it was previously reported that a small magnetic field seems to determine the chirality of ferromagnetic domain wall after the high temperature phase transition from the paramagnetic state[10], it was suggested here that the chirality is preserved in the course of low temperature phase transition from the helimagnetic phase.

To confirm the chirality memory effect of the ferromagnetic domain walls, we investigated the  $H^c_{80K}$  dependence of  $\rho^{2f}_{\text{asym}}$ . In Figs. 3(c) and 3(d), we plot  $\rho^{2f}_{\text{asym}}$  measured after the annealing process normalized by that before the annealing process ( $\rho^{2f}_{\text{asym}0}$ ) as a function of  $H^c_{80K}$ , compared with the linear resistivity in magnetic fields parallel to the  $c$ -axis. The linear resistivity showed hysteretic behavior. The initial state of the measurement was zero magnetic field just after heating from the helimagnetic state. The resistivity was relatively large at the initial state and decreased with the magnetic field (circles). After the application of a large magnetic field, the resistivity showed a butterfly type hysteresis loop (triangles and squares) and was smaller than the initial resistivity. These features indicate that the magnetic domain walls present at the initial state increased the resistivity, which disappeared above 0.4 T. Importantly,  $\rho^{2f}_{\text{asym}} / \rho^{2f}_{\text{asym}0}$  was quenched at almost the same magnetic field as shown in Fig. 3(d). This strongly supports the scenario that the

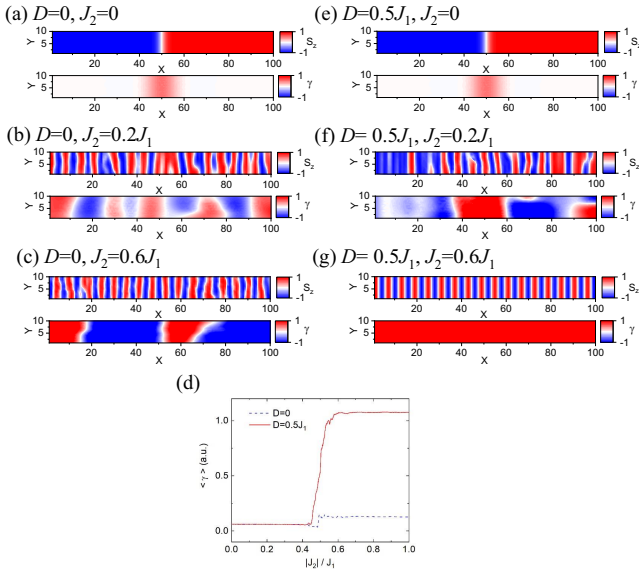


FIG. 4. Numerical simulations of the memory effect. (a)-(c) The snapshots of  $z$ -axis spin moment  $S_z$  and chirality  $\gamma = (\vec{S} \times \nabla \vec{S})_x$  in increasing  $J_2$  at (a)  $J_2=0$ , (b)  $J_2=0.2J_1$ , and (c)  $J_2=0.6J_1$ . In these cases, Dzyaloshinskii-Moriya interaction is absent. (d)  $J_2$  dependence of the chirality for  $D=0$  and  $D=0.5J_1$ . Here  $D$  is the maximum of the position dependent DM interaction  $D_i$ . They are the averages of 100 samples in the presence of random magnetic field, which corresponds to the thermal fluctuation. (e)-(g) The snapshots of  $S_z$  and  $\gamma$  at (e)  $J_2=0$ , (f)  $J_2=0.2J_1$ , and (g)  $J_2=0.6J_1$  in the presence of  $D=0.5J_1$ .

magnetic domain walls memorized the chiral information in the FMI phase.

Finally, we show numerical simulations of the chirality memory effect. We employed two-dimensional  $100 \times 10$  spin system in the  $xy$  plane with Hamiltonian

$$\mathcal{H} = - \sum_{nn} J_1 \vec{S}_i \cdot \vec{S}_j + \sum_{nnn} J_2 \vec{S}_i \cdot \vec{S}_j - \sum_i (K_x S_{ix}^2 + K_z S_{iz}^2), \quad (1)$$

where the  $J_1$  is the ferromagnetic exchange interaction between the nearest neighbor (nn) and  $J_2$  is the antiferromagnetic exchange interaction between the next nearest neighbor (nnn) spin pairs along the  $x$ -direction, which stabilizes the helical spin structure with the propagation vector along the  $x$ -axis.  $K_z$  ( $K_x$ ) is the anisotropic energy of the easy  $z$  (hard  $x$ ) axis. With this spin system, we numerically show how the chirality of the ferromagnetic domain wall is transmitted to that of a helimagnetic state. We prepare ferromagnetic state with a Bloch-type domain wall along the  $y$ -axis as the initial state (Fig. 4(a)). By means of the Landau-Lifshitz-Gilbert equation, we numerically calculate the spin dynamics in the course of the ferromagnetic-to-helimagnetic phase transition with increasing the value of the  $J_2$  at a rate of  $0.1J_1/\text{ns}$ . We also introduce the fluctuating random magnetic field, which represents thermal fluctu-

ation. The details in the numerical simulation are the same as those in a literature[28]. Figures 4(a)-4(c) exemplify snapshots of the magnetization component ( $S_z$ ) and the chirality ( $\gamma = (\vec{S} \times \nabla \vec{S})_x$ ). One can see the gradual evolution of helical structure. When  $J_2 = 0.6J_1$ , the helimagnetic state is realized. However, we have found that the chirality of the obtained helical state does not follow that of the magnetic domain wall but is governed by the random field. In many cases, there are multiple chirality domains. The dashed line in Fig. 4(d) represents the  $J_2$  dependence of the chirality that is averaged over 100 samples. Even in the helical state, the average of chirality is almost vanished because of the randomness. Therefore, in order to explain the chirality memory effect, one must consider some additional effect. The most plausible possibility is the interplay with lattice degree of freedom. Chiral magnetic structures are expected to induce chiral strain owing to the inverse effect of Dzyaloshinskii-Moriya (DM) interaction. Because lattice dynamics is generally slow compared with spin dynamics, the strain remains nearly static in the course of the first-order ferromagnetic-helimagnetic transition. Such static strain should give rise to local DM interaction on the magnetic system. For these reasons, we added

$$H_{DM} = \sum_{nnx} D_i (\vec{S}_i \times \vec{S}_{i+x})_x \quad (2)$$

to the spin Hamiltonian. Here summation runs over nearest-neighbor spin pairs along the  $x$ -axis.  $D_i$  is position-dependent DM interaction proportional to the local chirality of the initial state. As shown in Fig. 4(e)-4(g), the helimagnetic state evolves from the position of the initial domain wall in this case. In this sample, the single helimagnetic domain is realized and the chirality is the same as that of the initial ferromagnetic domain wall. While there exist chirality domain walls in some other samples even in the presence of DM interaction, the number becomes smaller and the chirality tends to follow that of the initial state irrespective of samples. The solid line in Fig. 4(d) represents the  $J_2$  dependence of averaged chirality in the presence of local DM interaction. One can see that finite chirality evolves around  $J_2 = 0.5J_1$ . Thus, this calculation demonstrates that the chirality of ferromagnetic domain wall transferred to that of helimagnetic structure with the help of local chiral strain and resultant DM interaction.

In conclusion, we have demonstrated a chirality memory effect of ferromagnetic domain walls. The chirality of the helical magnetic structure is preserved even after annealing in the high-temperature ferromagnetic state at zero field. As visualized by the Lorentz electron microscopy study[10], the ferromagnetic state has Bloch-type chiral magnetic domain walls at zero magnetic field. The numerical calculation indicates a possible role of chiral lattice distortion around the domain walls for the chirality memory effect. While the possibility of polarization memory effect owing to the magnetic domain wall in a multiferroic was previously suggested[21],

the present result more clearly shows, based on the experimental result of magnetic field application along the easy axis in the ferromagnetic state, that the Bloch-type domain walls are responsible for the memory effect in the case of MnP. This suggests that the magnetic domain walls work as small chiral nuclei in the nonchiral phase, which are important in determining the chirality after the first-order nonchiral-chiral phase transition. This phenomenology seems to be applicable to general chirality problems. Chirality is also valid in topological defects and dislocations[29]. This work suggests the vital role of such local chiralities in achiral states.

The crystal growth was carried out by joint research in the Institute for Solid State Physics, The University

of Tokyo with the help of R. Ishii and Z. Hiroi. The fabrication of the sample device was carried out partly by collaborative research in the Cooperative Research and Development Center for Advanced Materials, Institute of Materials Research, Tohoku University with the help of K. Takanashi and T. Seki. This work was supported in part by JSPS KAKENHI grant numbers JP16H04008, JP17H05176, JP18K13494, JP19H05600, and JP20K03828, the JST ERATO Spin Quantum Rectification Project (JPMJER1402), PRESTO grant number JPMJPR19L6, the Murata Science Foundation and the Mitsubishi foundation. N.J. is supported by a JSPS fellowship (No. JP19J11151).

- 
- [1] M. Avalos, R. Babiano, P. Cintas, J. L. Jiménez, J. C. Palacios, and L. D. Barron, *Chem. Rev.* **98**, 2391 (1998).
- [2] B. L. Feringa and R. A. van Delden, *Angew. Chem. Int. Ed.* **38**, 3418 (1999).
- [3] S. Mühlbauer, B. Binz, F. Jonietz, C. Pfleiderer, A. Rosch, A. Neubauer, R. Georgii, and P. Böni, *Science* **323**, 915 (2009).
- [4] X. Yu, Y. Onose, N. Kanazawa, J. Park, J. Han, Y. Matsui, N. Nagaosa, and Y. Tokura, *Nature* **465**, 901 (2010).
- [5] Y. Togawa, T. Koyama, K. Takayanagi, S. Mori, Y. Kousaka, J. Akimitsu, S. Nishihara, K. Inoue, A. S. Ovchinnikov, and J. Kishine, *Phys. Rev. Lett.* **108**, 107202 (2012).
- [6] E. E. Huber and D. H. Ridgley, *Phys. Rev.* **135**, A1033 (1964).
- [7] T. Yamazaki, Y. Tabata, T. Waki, T. J. Sato, M. Matsuura, K. Ohoyama, M. Yokoyama, and H. Nakamura, *J. Phys. Soc. Jpn.* **83**, 054711 (2014).
- [8] G. P. Felcher, *J. Appl. Phys.* **37**, 1056 (1966).
- [9] R. M. Moon, *J. Appl. Phys.* **53**, 1956 (1982).
- [10] T. Koyama, S. Yano, Y. Togawa, Y. Kousaka, S. Mori, K. Inoue, J. Kishine, and J. Akimitsu, *J. Phys. Soc. Jpn.* **81**, 043701 (2012).
- [11] Y. Shiomi, S. Iguchi, and Y. Tokura, *Phys. Rev. B* **86**, 180404(R) (2012).
- [12] M. S. Reis, R. M. Rubinger, N. A. Sobolev, M. A. Valente, K. Yamada, K. Sato, Y. Todate, A. Bouravleuv, P. J. von Ranke, and S. Gama, *Phys. Rev. B* **77**, 104439 (2008).
- [13] A. Zieba, C. C. Becerra, H. Fjellvåg, N. F. Oliveira, and A. Kjekshus, *Phys. Rev. B* **46**, 3380 (1992).
- [14] K. Taniguchi, N. Abe, S. Ohtani, and T. Arima, *Phys. Rev. Lett.* **102**, 147201 (2009).
- [15] Y. M. Xie, H. Zang, W. D. Ceng, H. Y. Wu, and C. C. Wang, *Appl. Phys. Lett.* **113**, 082906 (2018).
- [16] W. B. Wu, D. J. Huang, J. Okamoto, S. W. Huang, Y. Sekio, T. Kimura, and C. T. Chen, *Phys. Rev. B* **81**, 172409 (2010).
- [17] C. De and A. Sundaresan, *Appl. Phys. Lett.* **107**, 052902 (2015).
- [18] T. Nakajima, S. Mitsuda, H. Yamazaki, and M. Matsuura, *J. Phys. Soc. Jpn.* **82**, 024706 (2013).
- [19] S. Mitsuda, T. Nakajima, M. Yamano, K. Takahashi, H. Yamazaki, K. Masuda, Y. Kaneko, N. Terada, K. Prokes, and K. Kiefer, *Physica B: Condens. Matter* **404**, 2532 (2009).
- [20] C. De, R. Bag, S. Singh, and A. Sundaresan, *Phys. Rev. B* **100**, 104407 (2019).
- [21] J. Beilsten-Edmands, S. J. Magorrian, F. R. Foronda, D. Prabhakaran, P. G. Radaelli, and R. D. Johnson, *Phys. Rev. B* **94**, 144411 (2016).
- [22] See Supplemental Material at [URL will be inserted by publisher] for the additional information.
- [23] N. Jiang, Y. Nii, H. Arisawa, E. Saitoh, and Y. Onose, *Nat. Commun.* **11**, 1601 (2020).
- [24] G. L. J. A. Rikken, J. Fölling, and P. Wyder, *Phys. Rev. Lett.* **87**, 236602 (2001).
- [25] T. Yokouchi, N. Kanazawa, A. Kikkawa, D. Morikawa, K. Shibata, T. Arima, Y. Taguchi, F. Kagawa, and Y. Tokura, *Nat. Commun.* **8**, 866 (2017).
- [26] R. Aoki, Y. Kousaka, and Y. Togawa, *Phys. Rev. Lett.* **122**, 057206 (2019).
- [27] A. Inui, R. Aoki, Y. Nishiue, K. Shiota, Y. Kousaka, H. Shishido, D. Hirobe, M. Suda, J.-i. Ohe, J.-i. Kishine, H. M. Yamamoto, and Y. Togawa, *Phys. Rev. Lett.* **124**, 166602 (2020).
- [28] J. Ohe and Y. Onose, *Appl. Phys. Lett.* **118**, 042407 (2021).
- [29] P. M. Chaikin and T. C. Lubensky, *Principles of Condensed Matter Physics* (Cambridge University Press, 2000).